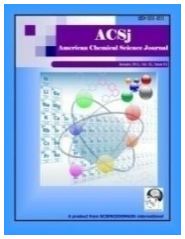

American Chemical Science Journal
4(3): 298-325, 2014

SCIENCEDOMAIN *international*
www.sciencedomain.org

Analysis of Thermodynamics, Kinetics and Equilibrium Isotherm on Fe^{3+}/Fe^{2+} Adsorption onto Palm Kernel Shell Activated Carbon (PKSAC): A Low-cost Adsorbent

Uzoije Atulegwu Patrick[1*], Uche Cosmas Chinedu[1] and Ashiegbu Darlington[1]

[1]Department of Environmental Technology. Federal University of Technology Owerri Imo State, Nigeria.

Authors' contributions

This work was carried out in collaboration between all authors. Author UAP designed the study, performed the statistical analysis, wrote the protocol, and wrote the first draft of the manuscript. Authors UCC and AD managed the analyses of the study. Author UAP managed the literature searches. All authors read and approved the final manuscript.

Original Research Article

Received 26th September 2013
Accepted 12th November 2013
Published 15th January 2014

ABSTRACT

Adsorption of Fe^{3+}/Fe^{2+} from a polluted shallow well water onto a palm kernel shell activated carbon (PKSAC) has been studied. Batch experiment was adopted to study the Removal efficiency of Fe^{3+}/Fe^{2+} on varying contact time, temperature, adsorbent loading and concentrations. Equilibrium isotherm and kinetic were also studied. Removal efficiency progressed with contact time till the peak adsorption time of 100 minutes when the efficiency remained at equilibrium. Also, removal efficiency got to equilibrium at the peak values of 80ºC, 4.8g and 12.5mg/l for temperature, adsorbent loading and concentration variations respectively. The adsorption isotherm models fitted the isotherm data got at 25ºC, 40ºC and 80ºC in this order; Langmuir > Temkin>Freunlich. The dimensionless separation factor of 0.012, 0.017 and 0.015 for 25ºC, 40ºC and 80ºC respectively confirmed favorable adsorption of Fe^{3+}/Fe^{2+} on the PKSAC adsorbent. Langmuir adsorption capacity increased from 203.9mg $Fe^{3+}/Fe^{2+/}$g to 389.3 mg $Fe^{3+}/Fe^{2+/}$g when the temperature increased from 25ºC to 40ºC but decreased to 308.1 mg $Fe^{3+}/Fe^{2+/}$g at

**Corresponding author: Email: patuzong@yahoo.com.hk;*

temperature of 80ºC. The kinetic models described the kinetic study data got at 25ºC, 40ºC and 80ºC as follows; power-function>second-order>Elovick>intra-diffusion>first-order kinetics. Mass transfer through liquid film diffusion controlled the adsorption of Fe^{3+}/Fe^{2+} onto PKSAC. Negative values of the Thermodynamic parameters ($\Delta \boldsymbol{G^o}$, $\Delta \boldsymbol{H^o}$ and $\Delta \boldsymbol{S^o}$) got at various temperature values showed favorability of adsorption of $Fe^{3+/}Fe^{2+}$ onto PKSAC. It is therefore concluded that PKSAC removed $Fe^{3+/}Fe^{2+}$ from aqueous solution.

Keywords: Adsorption; Fe^{3+}/Fe^{2+}; isotherm models; equilibrium; kinetic models; removal efficiency; thermodynamics.

1. INTRODUCTION

Iron is a major constituent of the earthcrust [1]. 5% of average crustal abundance is iron. Depending on the sediment transport, the geochemical history and rock from which the soil was formed, the iron content is of the range of between 0.5% and 5% [2]. The iron mainly occurs in natural form as iron minerals which include; siderite, hematite, goethite and magnetite. The weathering releases the iron in the water. That is the natural pathway. Iron can as well find its way into the water through anthropogenic means. The most common means are through industrial effluent, acid-mining drainage, sewage and landfill leachate [3]. There are two forms of iron in water; ferric ion (Fe^{3+}) and ferrous iron (Fe^{2+}). In surface water the ferrous iron dominates due to it soluble nature while in ground water, the fate of iron depends on the prevailing conditions. Under the condition of reduction reaction, ferrous iron is prevalent while ferric iron dominates under oxidation condition [4]. The transition from ferrous to ferric iron in the presence of oxygen explains why ground water sufficiently polluted by ferrous iron gradually turns brownish on exposure to atmosphere. The ferrous iron is oxidized to ferric iron by the atmospheric oxygen. The insolubility tendency of ferric iron, couple with its ability to form complexes makes it susceptible to precipitation hence the reddish brown sediment. The reaction is as follows:

$$4Fe + 3O_2 + 6H_2O \rightarrow 4Fe^{3+} + 12OH^- \rightarrow 4Fe(OH)_3 \text{ or } 4Fe(OH) + 4\ H_2O$$

Iron is a dietary need either in binary or tertiary form for both micro and macro organisms. Iron is essential for nitrogen binding and nitrate reduction processes, which when in scarce can limit growths of phytoplankton growth. Soil types containing high or low concentration of water soluble iron portends growth problems to plants [5]. In human being, iron forms chelation complexes which encourage production of hemoglobin and in turn binds and releases oxygen during breathing [6]. When in deficits iron could lead to anemia, causing tiredness, headaches and loss of concentration [7]. Presence of iron in drinking water at low concentration is not considered a health problem. Small iron concentration is essential for human health but over dosage of iron gives drinking water unpleasant taste. It also makes vegetables cooked with iron–contaminated water appear unappetizing with dark appearance [8]. Iron bacteria, does not pose much health problem but leave behind reddish- brown slime clogs to plumbing materials as they live in the iron just to survive. This equally causes an offensive odor. Presence of These bacteria is also obvious in the slimy coating of the pipe, staining of lundary materials and toilet tanks [7]. To human being, iron concentration in drinking water beyond world health organization (WHO) recommended limit of 0.3mg/l or at unbearably high level could lead to adverse health effects which include; conjunctivitis, siderosis etc [6]. With these seeming environmental problems, researchers have adopted traditional methods to remove iron from drinking water. These methods comprise; the

reverse osmosis, water softener(ion exchange).aeration, oxidizing filter, chlorination and filter, Fenton etc [9,10,11,12,13,14,15]. Adsorption techniques using synthetic adsorbents have yielded significant results [16,17]. Some of these methods are no doubt efficient but expensive with adverse after effects [18]. Chlorination has yielded appreciable result in iron removal, but could be harmful to health due to poor handling. Several researchers have equally explored various adsorption techniques on iron and heavy metal removal in drinking water using adsorbent materials. [19] Used zoelite, kaolinite and bentonite for such treatment. Although, it has been proven that the high cost of these adsorbents has being a challenge. In the light of this, researchers made use of agricultural waste and other available low cost adsorbent materials for remediation. This yielded good results. For example, [20,21,22,23] have shown the effectiveness of agricultural waste and other organic solid waste adsorbents in removing varying concentrations of heavy metals, dye and organic pollutants. Low cost adsorbents have successfully removed types of dye species [22]. [24,25,26,27] substantially reduced high concentrations of Hazardous brilliant blue dye, Azo dye(Metani Yellow), crystal violet dye and Reactofix golden yellow 3-RFN in drinking water using bottom ash and de-oiled soya, wheat-husk,. Similarly, [28] explored biosorption technique to treat nickel contaminated drinking water using algae (oedogonium hatei) as adsorbent. Palm kernel shell activated carbon which is available and affordable has in resent time been used by several researchers to remove varying concentration degrees of heavy metal in drinking water. Emmanuel et al. [29] removed Cd^{2+} and Pb^{+} from a heavy metal polluted wastewater .Ademuliyi and David-West 2012 [30] researched and proved that palm kernel shell activated carbon can reduce to the barest minimum the following heavy metal from waste stream ; Cr^{2+}, Cu^{2+}, Ni^{2+}, Pb^{2+}, Fe^{2+}, and Zn^{2+}. Other researchers have stressed on the availability , affordability and effectiveness of palm kernel activated shell to remove metal pollutant from drinking water [21,18,6,9], but on study has robustly treated remediation of Iron pollution in drinking water using palm kernel shell activated carbon. This study investigated the effectiveness of palm kernel shell activated carbon in removing iron ion form drinking water . The study also measured the adsorption isotherms and kinetics models of the work. To assess the fitness of the data to various isotherm and kinetic models.

2. MATERIALS AND METH ODS

2.1 Preparation of Activation Carbon Fiber and Fiber Characterization

The palm kernel shell of the lignocellulosic material fiber was used to produce high quality activated carbon for this study. The palm kernel shell was obtained from an palm oil processing mill at Umuagwo-Ohaji Owerri Imo state south- Easther Nigeria. The material was carbonized and activated in a furnace of temperatures of 600ºC and 800ºC respectively. [31,32,33] published in details the preparation, carbonization and activation procedures of the material.

2.2 Characterization of Palm Kernel Shell Activated Carbon (PKSAC)

A sample of the PKSAC was used to measure the following properties; Conductivity, Ph, Percentage yield, Bulk density, Ash content, Moisture content , Carbon hardness and Porosity. Ph and moisture content values of the activated carbon were determined using standard test methods of ASTM D 3838-80 (ASTM 1996) and ASTM D 2867-91 (ASTM 1991) respectively. Tampering procedure as proposed by [34] was adopted to find out the

bulk density. Percentage yield, ash content, conductivity, and carbon hardness were determined according to procedures described by [35,36,37,38] respectively.

2.3 Characterization of the Shallow Well Water (SWW)

Random sampling method was adopted in the collection of SWW samples from seven shallow wells within Buguma city, Rivers state Nigeria. Each sample was analyzed for ph, phosphate(p), lead (pb), total dissolved solids(TDS), Conductivity(µs), Biological oxygen demand(BOD),Ph and iron ion . All the analysis were carried out using standard methods. The results of all the samples were averaged and presented in the table.

2.4 Adsorption Equilibrium Fe^{3+}/Fe^{2+}

To estimate the adsorption capacity of the adsorbent (PKSAC) through equilibrium time study, a batch adsorption equilibrium experiment was carried out. In this experiment, 500ml round bottom flask was used into which a solution of 100mg/l concentration of 200mg/l formed with 2.1g of the adsorbent was introduced. Also introduced was a 150ml of well water with an Fe^{3+}/Fe^{2+} concentration of 10mg/l. The PKSAC/SWW system was shaken at 260RPM at room temperature of 25ºC until adsorption equilibrium time was established. At this period, an aliquot from the flask was removed. The left-over PKSAC particles in the aliquot were filtered off using 0.43µm filter before it was analyzed for Fe^{3+}/Fe^{2+}. The amount adsorbed at equilibrium was calculated using the following model

$$\boldsymbol{q}_{e=\left(\frac{C_o - C_e}{m}\right)\boldsymbol{V}} \quad 1a$$

Where $\boldsymbol{C_o}$ $\boldsymbol{and}$ $\boldsymbol{C_e}$ represent the initial and final concentrations respectively. $\boldsymbol{C_e}$ Can as well be expressed as the concentration of the adsorbate, (Fe^{3+}/Fe^{2+}) remaining in solution at the point of equilibrium. V and m were defined as the volume of the SWW and m is the mass of adsorbent respectively. The capacity of the adsorbent to adsorb Fe^{3+}/Fe^{2+} was measured in percentage termed percentage removal and was expressed mathematically

$$\%\text{Removal} = \frac{C_o - C_t}{C_o}\boldsymbol{X100} \quad 1b$$

The experimental data were fitted into the classical Fraundlich, Langmuire amd Temkin adsorption models expressed in equations 2, 3 and 4 respectively.

2.4.1 Freundlich model

Freundlich model describes the multilayer adsorption process of adsorbate and affinity over a heterogeneous adsorbent surface. The adsorbent surface has adsorption sites onto which adsorbates are held by binding energies. Those with stronger binding energies are occupied first with an exponential decrease in the energy as adsorption completes. Freunlich model is expressed as follows:

$$\boldsymbol{q_e = K_F C_e^{1/n}} \ . \quad 2a$$

The nonlinearized form of equation 2a is converted into a linearized equation by taking natural log of both sides of equation 2a and it is given as follows:

$$\ln q_e = lnK_F + \frac{1}{n} lnC_e \quad (2b)$$

Where qe represents the adsorbate adsorbed at equilibrium, K_F is the Freunlich constant, 1/n is the heterogeneity factor. n measures the deviation from linearity of adsorption . n can still be described as a measure of adsorption intensity or surface heterogeneity. Adsorption surface becomes more heterogeneous as n value tends to zero [39]. Therefore various values of n describe the form the adsorption takes. n is measured in the range between 0 and 1. Adsorption is said to be linear if n=1. Adsorption is chemical if n<1 and physical if n>1

2.4.2 Langumir Model

Langumir model quantifies adsorption capacity of adsorbents of a homogeneous surface. Langumuir describes an adsorption process on a fixed or definite site which provides no lateral interaction between adsorbed molecules [40]. Langumir model described and adsorption surface with the following qualities (1) The adsorption surface must be homogeneous in nature. (2) each adsorption molecule must have equal Enthalpy and activation energies. (3) all the adsorption sites possess the same attraction to the adsorbing substance adsorption of substance onto such surface presupposes that the movement of adsorbed molecule from one site to another may be impossible [41,42,43]. With all these assumptions, langumir proposed the following model to predict the adsorption of aqueous substance in a monolayer pattern onto a solid surface.

The non-linear form of the model is as $q_e = \frac{q_{max} b C_e}{1 + bC_e}$ .. (3a)

The linearized form is expressed as $\frac{1}{q_e} = \frac{1}{q_{max}} + \frac{1}{K_L q_{max} C_e}$ (3b)

Where q_e and C_e remain as defined above while q_{max} and K_L are defined as the maximum adsorption and Langmuir constant respectively. Also, a dimensionless constant popularly know as separation factor R_L proposed by Webber and Chakkravorti, [43] further describes the adsorption capacity of the adsorbent. Webber and Chakkravorti, [43] mathematically expressed R_L as

$$R_L = \frac{1}{1 + K_L C_o} \quad (3c)$$

Where K_L is as defined above and Co refers to as the initial concentration of the adsorbate. Values of R_L provides important information about the nature of adsorption and that is expressed as follows; RL < 1 means favourable adsorption, R_L > 1 refers to unfavourable adsorption, R_L = 1 suggests linear adsorption and R_L=0 confirms an irreversible adsorption. Adsorption is more favourable as R_L tends to lower value.

2.4.3 Temkin model

Temkin isotherm model describes the adsorbate-adsorbent interaction and uniform distribution of binding energies between the adsorbing molecules and the surface adsorbent during adsorption processes. The model also assumes the heat of adsorption which is a function of temperature varying linearly with coverage rather than logarithmically. Temkin model is mathematically expressed in non-linear and linear form as shown in equations 4a and 4b respectively

$$q_e = \frac{RT}{b_T} lnA_T C_e \quad (4a)$$

$$q_e = \frac{RT}{b_T} lnA_T + \frac{RT}{b_T} lnC_e \quad (4b)$$

Where A_T and b_T are described as maximum binding energy and heat of biosorption respectively. Heat of biosorption suggests adsorption potentials or intensity of adsorption of the adsorbent.

2.5 Adsorption kinetic Studies

To study the equilibrium time and kinetics of adsorption of Fe^{3+}/Fe^{2+} onto PKSAC, batch process similar to that adopted in the equilibrium study was employed. For the kinetic study, adsorption of Fe^{3+}/Fe^{2+} was studied at interval of 10 minutes up to 120 minutes. Adsorption kinetic studies were also carried out at varying temperature values of 25ºC, 40ºC and 60ºC, different initial SWW concentrations of 2.8mg/l, 5.8mg/l and 10.92mg/l and different adsorbent weight of 2.1g, 3.5g and 5.1g. The study at interval of 10 minutes implies that samples were collected from the supernatant at the end of every 10 minutes of adsorption process for Fe^{3+}/Fe^{2+} analysis using Atomic Absorption spectrometer. The amount of Fe^{3+}/Fe^{2+} adsorbed onto the PKSAC at any point in time was calculated using the following equation.

$$q_t = \frac{(C_o - C_t)V}{M} \quad (5)$$

Where qt referred to Fe^{3+}/Fe^{2+} adsorbed onto the PKSAC absorbent per time , C_t is Fe^{3+}/Fe^{2+} remaining in solution per time of adsorption , V and M were as defined above. To interpret the time dependent experimental data the following kinetic models were considered and were mathematically expressed as follows;

2.5.1 Psuedo-first order equation

$$\frac{dq_t}{dt} = K_1(q_e - q_t) \quad (6a)$$

After separating the variables and integration, equation 6a is gives

$$log(q_e - q_t) = logq_e + \frac{K_1}{2.303} t \quad (6b)$$

q_e and q_t have been defined above. K_1 represents the Psuedo-first order reaction constant while t is the time of adsorption

2.5.2 Second order kinetic

$$\frac{dq_t}{dt} = K_2(q_e - q_t)^2 \quad (7a)$$

Equation 7a was linearized after separating the variables and integrating the variable to give

$$\frac{t}{q_e} = \left(\frac{1}{K_2 q_e^2}\right) + \left(\frac{1}{q_t}\right) t \quad (7b)$$

2.5.2 Power function

$$q_t = at^b \quad (8a)$$

Power function adsorption kinetic equation describes the relationship between uptake of Fe^{3+} onto the PKSAC and time of adsorption. ''a'' which is the most important power function constants showed the adsorption rate of Fe^{3+}/Fe^{2+} .'' b'' is also a constant while all other variables remained as described . The power function is linearized by taking log of both sides of equation to give

$$logq_t = loga + blogt \quad (8b)$$

2.5.3 Elovich kinetic Equation; the model was expressed in non-linear form as follows;

$$\frac{dq_t}{dt} = aexp(-\beta q_t) \quad (9a)$$

Equation 9a is simplified by separating the variables, integrating and applying the boundary conditions;

$$q_t = 0 \; at \; t = 0 \; and \; q_t = q_t \; at \; t = t \text{ to give } q_t = \frac{1}{\beta}\ln \alpha\beta + \frac{1}{\beta}\ln t \quad (9b)$$

α' represents initial adsorption rate (mg/g min) while β is the desorption constant (g/mg). Also [46] reported that β is related to the extent of coverage of the adsorbate onto the adsorbent.

2.5.4 Intra-particle diffusion

Adsorption process takes place in two major stages; external mass transfer and intra-particle diffusion. The intra-particle diffusion is expressed by this model;

$$q_t = K_t t^{0.5} \quad (10a)$$

Where K_t decides the adsorption capacity of the adsorbent. K_t is expressed as follows;

$$K_t = \frac{6q_e}{R}\sqrt{\frac{D}{\pi}} \quad (10b)$$

From equation 10b, K_t is proportional to $q_{e \; and \; D^{0.5}}$ suggesting that K_t increases with increasing adsorption equilibrium and the intra-particle diffusion D. K_t also finds out the adsorption capacity. Equations 10 a and b are applied when intra- particle diffusion controls the adsorption.

For the external mass transfer stage (that is the migration of solute molecule from the liquid phase up to the solid phase) a model referred to as liquid diffusion model is employed and is expressed as

$$ln(1-\alpha) = K_t t \quad (10c)$$

Where α is the fractional attainment to equilibrium (FATE). FATE is expressed as $\alpha = \frac{M_t}{M_\infty}$. M_t represents the concentration of iron ion at time t, while M_∞ is the concentration of iron ion

at infinity or equilibrium. High values of $\boldsymbol{\alpha}$ suggests quick attainment of adsorption process to equilibrium. If the plot of $\boldsymbol{ln(1-\alpha)\, Vs\, t}$ gives a linear curve with out passing through the origin, it is sufficient to conclude that the diffusion of iron ion under study gets to the adsorbent (PKSAC) through the liquid film boundary surrounding the adsorbent. This implies that the external particle diffusion mechanism predominates. It further suggests that the iron ion particle diffused the PKSAC through the liquid film before the intra-particle diffusion stage takes place.

2.6 Thermodynamic Process

The study was carried out to determine the following thermodynamic changes; activation energy, changes in Gibb-free energy(∆Go), Enthalpy(∆H) and Entropy (∆S).

2.6.1 The activation energy was studied at different temperature values using the arrhenius model

$$\boldsymbol{K_{ad} = Ae^{-E_a/RT}} \tag{11a}$$

While A is the Arrhenius constant, Ea is referred to as activation energy of adsorption ($KJmol^{-1}$) . Ea is the minimum energy value required to initiate chemical adsorption. R and T are the gas constant (8.314 J/mol/K) and absolute temperature (k) respectively, $\boldsymbol{K_{ad}}$ is adsorption rate constant.

Natural log was taken on both sides of 11a to form a straight line equation expressed as

$$\boldsymbol{lnK_{ad} = lnA - \frac{E_a}{RT}} \tag{11b}$$

2.6.2 Gibb- free Energy of Adsorption (∆G) was expressed as follows

$$\boldsymbol{\Delta G = -RTlnK_L} \tag{12}$$

Gibbs free energy is an available useful energy that can do useful work in an adsorption process [39]. Gibb free energy determines levels of adsorption processes. For instance, negative values of ∆G show the feasibility of adsorption [47]. Spontaneity of adsorption decides between ∆G and temperature. In that light, decrease in the values of ∆G with increasing temperature marks the spontaneity of adsorption at higher temperature[48].

Enthalpy change describes the heat of adsorption . The extent of Enthalpy of adsorption decides the strength of binding energy of the adsorbate onto the adsorbent surface. If the Enthalpy of adsorption is negative the binding strength of the adsorbate on the adsorbent increases. Changes in Enthalpy (∆H) at different temperature values were determined graphically using the following equation.

$$\boldsymbol{\frac{\Delta G^o}{T} = \frac{\Delta H^o}{T} - \Delta S^o} \tag{13a}$$

While the Enthropy, $\boldsymbol{\Delta S^o}$ was obtained at various temperature values using the transformed version of equation 13 stated as

$$\boldsymbol{\Delta S^o = \frac{\Delta H^o - \Delta G^o}{T}} \tag{13b}$$

In this respect, the slope and the intercept Values of Van't Hoff plot of $\frac{\Delta G^o}{T} Vs\ T$ gave the values of Enthalpy. The endothermic nature of the process is confirmed by the positive values of ΔH^o while the exothermic process indicated by the negative Enthalpy value ($-\Delta H^o$) confirms that increase in temperature does not support adsorption [42] good affinity of adsorbate (Fe^{3+}/Fe^{2+}) towards the adsorbent is revealed by the positive value of ΔS^o [43].

3. RESULTS AND DISCUSSIONS

3.1 Characterization of Adsorbent

The results of the Textural characteristics of the adsorbent, PKSAC were shown in Table 1. The values of the analysis were virtually in line with the results obtained by other researchers. There were slight differences between values of bulk density (0.8332 g/cm3) and % as h(6.435) content obtained by Ademiluyi and David-West [30] from the present study. The disparity in values could be attributed to difference in species of the palm fruits.

Table 1. Textural Characteristic of the Adsorbent

Parameter	Values
Ph	6.48
%moisture	6.73
%yield	30.35
Bulk density(g/cm^3)	0.65
%Ash content	5.01
Conductivity(µs/cm)	36.11
%Carbon hardness	69.87
Porosity	0.39

3.2 Characteristics of the Well Water

The results of the physic-chemical properties of the water sample were show on Table 2. The results indicated that the sample values were within WHO drinking water standards except the iron concentration and conductivity which exceeded the standard. Concentration of iron was high while that of conductivity exceeded WHO standard slightly. The high iron content of the water sample is a source of concern to the users of this water. With the value of iron at 10.92 mg/l the water sample exceeded the WHO standard of 0.3 mg/l hence the need for its removal. The slight increase in the conductivity value could be as a result of high iron content of the water sample [49].

Table 2. Physiochemical Properties of the Water Sample

Parameter(mg/l)	Values	WHO limits
Pb	0.03	0.05
P043-	1.95	2.45
TDS	125	250
BOD	37.01	40
Ph	6.8	6.5-8.5
Fe	10.90	0.3
Conductivity(µs/cm)	110	100

3.3 Percentage Removal of Fe^{3+}/Fe^{2+}

3.3.1 Effects of contact time

The time effects of percentage removal of Fe^{3+}/Fe^{2+} were evaluated at varying periods and the trend of variation was illustrated in Fig. 1. The efficiency varied directly with time until at a point when removal became constant with time in all the study conditions. It was observed from the result that the rate of removal was generally rapid at the time lag of 0-80 minutes and thereafter became constant as the time progressed . This could be attributed to the fact that the adsorption sites of the adsorbents were saturated with the adsorbates at adsorption periods beyond 80 minutes. Oladoja et al. [50] achieved saturation of methelene blue dye adsorption on ground palm kernel coat adsorbent at 68 minutes, while saturations of adsorption of Cu^{2+}, Ni^{+},Cr^{3+}, Zn^{2+} and pb^{2+} on palm kernel adsorbent occurred at 59, 63, 54, 73 and 72 minutes respectively [52]. The trends of Fe^{3+}/Fe^{2+} removal were equally in agreement with the study of palm kernel shell charcoal [39] where adsorption of Cd^{2+} and Pb^{2+} on palm kernel activated adsorbents were compared. The study of [43] on the adsorption of Pb^{2+} and Cr^{2+} on the palm kernel shell activated carbon also corroborated this work.

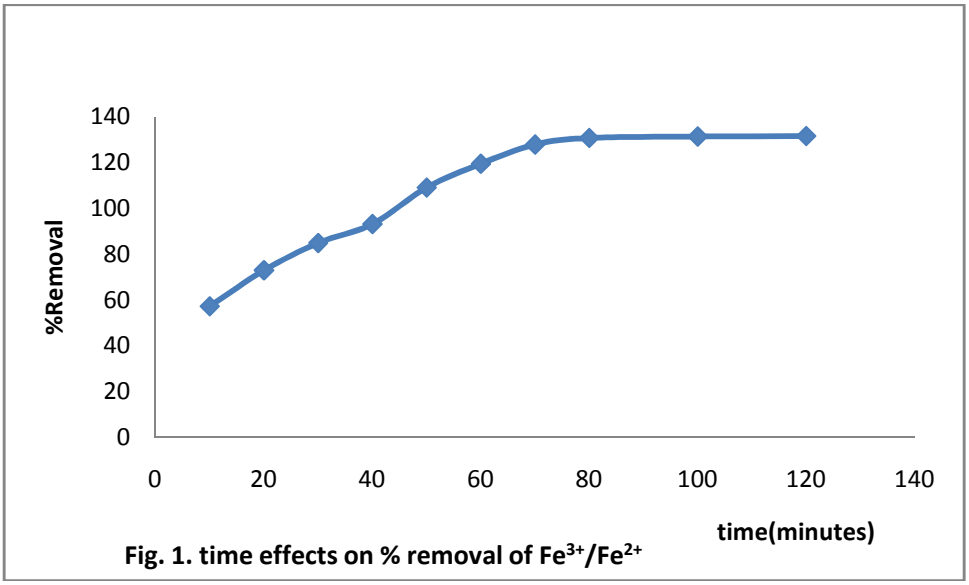

Fig. 1. time effects on % removal of Fe^{3+}/Fe^{2+}

3.3. 2 Effects of Temperature

Temperature is an important parameter in adsorption process. In this study, there was apparent variation in temperature with percentage removal of Fe^{3+}/Fe^{2+}. The variation assumed direct proportionality where temperature values increased as percentage removal also increased. As shown in Fig. 2, percentage removal increased linearly with temperature until at the temperature of 80ºC where the removal reached the plateau and remain constant. Temperature affects adsorption process in many ways. For instance increase in temperature increases the active sites of the adsorbents making the sites available for effective adsorption with concomitant removal of the adsorbate [44]. The same reason could be attributable to the pattern of adsorption observed in this study where adsorption of Fe^{3+}/Fe^{2+} from the well water sample onto PKSAC got to its saturated limit at 80ºC. Again

temperature increase which decreases the boundary layer thickness surrounding the adsorbent [45] could equally be attributed to this adsorption pattern. In this regard, the reduction in boundary layer thickness lowered the resistance of Fe^{3+}/Fe^{2+} mass transfer through the adsorbent(PKSAC) boundaries leading to more Fe^{3+}/Fe^{2+} adsorption. Another condition that facilitated Fe^{3+}/Fe^{2+} adsorption with temperature, could be attributed to the direct temperature effect with the mobility of adsorbate. In the light of this, temperature enhances the mobility of adsorbate from bulk solution towards the adsorbent surface [53,20]. Also, the point of equilibrium and possible adsorption decrease observed after 80ºC could suggest seeming solubility of Fe^{3+}/Fe^{2+} in the bulk solution [46]. Further temperature increase could lead to increase in oscillation energy of Fe^{3+}/Fe^{2+} resulting to Fe^{3+}/Fe^{2+} desorption from the adsorbent surface into the bulk solution [47]. This was equally substantiated by the observation that solubility of pollutants in bulk fluid determines its hydrophocity, implying that a highly hydrophobic substance, that is, a substance sparingly soluble shows greater affinity towards the adsorbate [48].

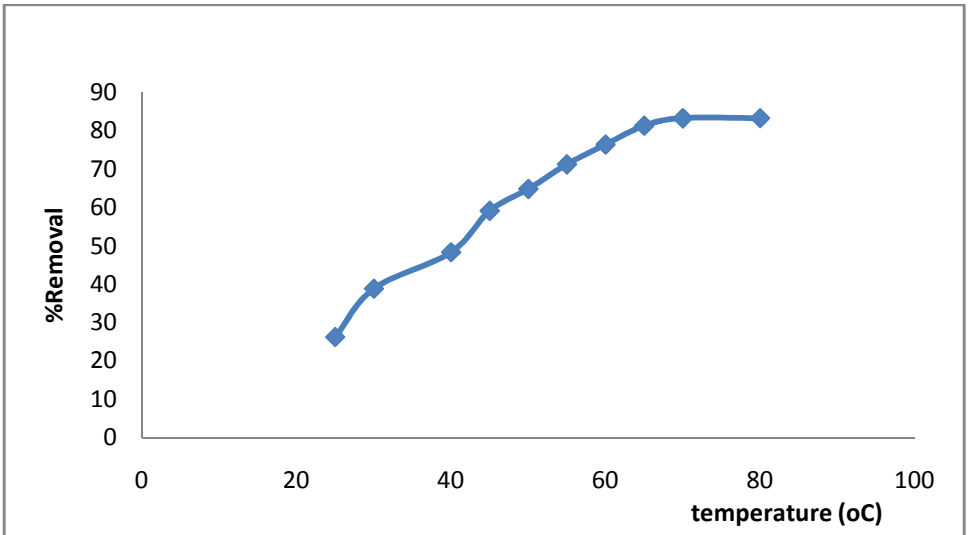

Fig. 2. Temperature effects on % removal of Fe^{3+}/Fe^{2+}

3.3.3 Effects of adsorbent loading

This work also studied the effects of adsorbent loading in relation to percentage removal. The study revealed that percentage removal increased with increasing adsorbent loading at the initial time but got to its equilibrium point as the process progressed. The results obtained from this study was shown in Fig. 3 the figure showed that percentage removal of Fe^{3+}/Fe^{2+} got to its equilibrium level at adsorbent loading of 4.8g. The initial trend of increase in percentage removal with increase in adsorbent loading could be attributed to provision of more surface areas as more adsorbent was loaded [49]. The prevailing condition resulted to more adsorption capacity of the adsorbent [54]. On the other hand, the percentage removal experienced an equilibrium state despite increase in adsorbent load. This condition could be attributed to large number of adsorbent sites having definite concentration of adsorbate [54,27]. The resultant effect is apparent reduction in Fe^{3+}/Fe^{2+} uptake and consequent decrease in percentage removal from the bulk solution [47]. Also, [55] corroborated the reason for the percentage removal equilibrium condition observed in this study to mean saturation of adsorption sites by Fe^{3+}/Fe^{2+} due to adsorbent load increase.

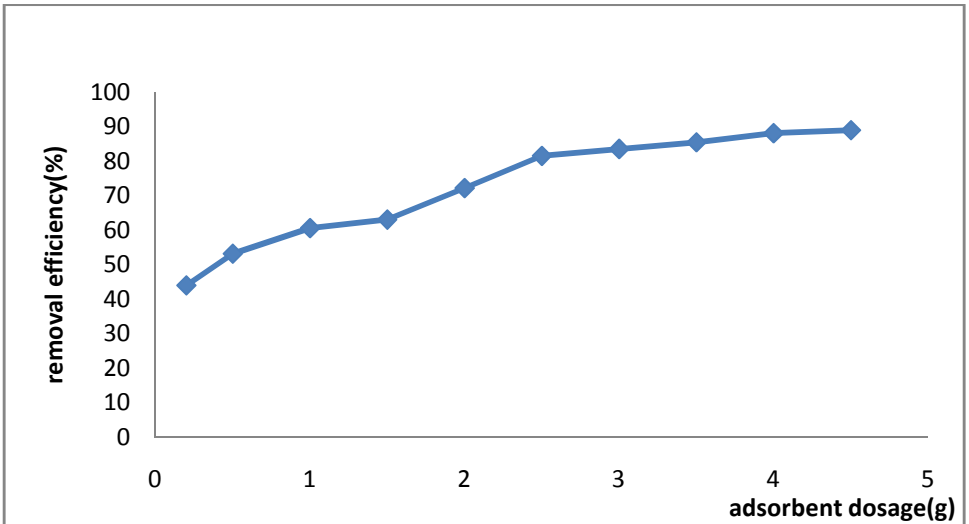

Fig. 3. Effects of adsorbent dosage on Fe^{3+}/Fe^{2+} removal

3.3.4 Effects of initial concentrations

Initial concentration of the polluted well water was varied to study its effects on the percentage removal of Fe^{3+}/Fe^{2+} from bulk solution. The result which was illustrated in Fig. 4 assumed opposite trend of percentage removal to that produced by temperature and adsorbent loading effects. In essence, the percentage removal decreased with increase in concentration of Fe^{3+}/Fe^{2+} in the bulk solution. Highest and lowest Percentage removals of 90% and 54% respectively at various 2mg/l and 12.5mg/l Fe^{3+}/Fe^{2+} concentrations were observed. However, the removal efficiency of Fe^{3+}/Fe^{2+} concentration of the polluted water (10.92mg/l) under study was equally observed at 70%. Emmanuel et al 2012 [20] achieved 88% and 87% removal efficiency of Pb+ and Cu^{2+} respectively using palm kernel shell carbon also, Ademuliyi and Davie-West 2012 [36] achieved 25%, 37% and 68% percentage removal of Cr^{3+}, Zn^{2+} and Ni^{2+} respectively using the same adsorbent. These further suggested that the adsorbent in use was capable of treating the well water of its high iron content. At equilibrium removal percentage of 54% With increased Fe^{3+}/Fe^{2+} concentration value of 12mg/l, the adsorption site of the adsorbent was saturated with Fe^{3+}/Fe^{2+}, rendering the removal efficiency of the adsorbent very low [55]. The study of [51,56-58] corroborated this observation.

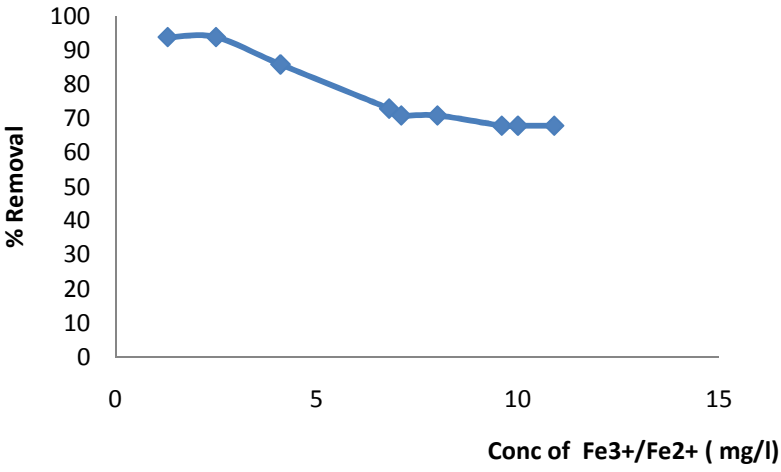

Fig. 4. Effects of concentrations on % removal

3.4 Adsorption Equilibrium Experiments

The data obtained from equilibrium experiment were calibrated using the following classical isotherm models; Langmuir, Fraunlich and Temkin .

3.4.1 Langmuir isotherm model

Results obtained from the equilibrium experiment were analyzed with Langmuir model shown in equation 3b. The suitability of the model to the equilibrium data was proved by making a linear plot of $\frac{1}{q_e}$ Vs $\frac{1}{C_e}$ with K_L and q_{max} representing the slope and intercept respectively. The curve was shown in Fig. 5.

The analysis which was carried out in three different temperature values of 25°C, 40°C and 80ºC showed reasonably high correlation, with correlation coefficient (R^2) values of 0.87, 0.95 and 0.90 respectively. According to Alzaydien 2009 [48], Langmuir model is said to have described an equilibrium data if the R^2 value is greater than 0.89. With this on ground, Langmuir model only fitted the equilibrium adsorption results of Fe^{3+}/Fe^{2+} onto PKSAC at 40ºC and 80ºC. This Also, confirmed the homogeneous nature of the PKSAC and the monolayer coverage of Fe^{3+}/Fe^{2+} onto the adsorbent [59] at 40 and 80ºC. Maximum adsorption capacities and Langmuir constants were obtained by calculation from the slope and intercept of the curve respectively and the results were displayed on Table 3. From the results, temperature have glaring effects on the maximum adsorption capacity of Fe^{3+}/Fe^{2+} onto PKSAC. The Maximum adsorption capacity values increased from 203.8 at 25ºC to 389.3 at 40ºC but decreased to 380.1 at 80ºC. The prevailing adsorption capacity distribution pattern with temperature showed that at high temperature of 80ºC adsorption of Fe^{3+}/fe^{2+} onto PKSAC experienced a decline with possible desorption as temperature increase progressed [60]. This trend confirms the exothermic nature of the adsorption [61]. It could also be attributed to oscillation energy increase and insolubility of Fe^{3+}/Fe^{2+} pollutants earlier discussed in the preceding sections.

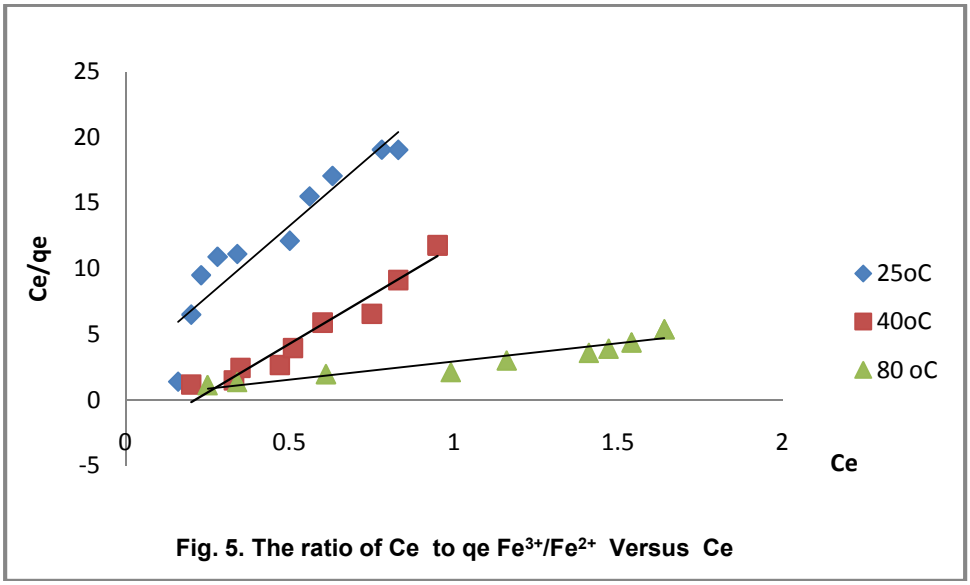

Fig. 5. The ratio of Ce to qe Fe^{3+}/Fe^{2+} Versus Ce

3.4.2 Separation factor

Favorability of Langmuir isotherm to equilibrium data was further investigated using a dimensionless constant popularly known as separation factor (RL) proposed by Webber and Chakkravorti 1974 [43] and mathematically expressed as shown in equation 3c. In this study, R_L was calculated with the Fe^{3+}/Fe^{2+} concentration of the well water (C_o) to be 10.92mg/l. R_L was calculated for various temperature values and the results were shown on Table 3. The result showed that RL values were less than 1 but greater than zero (0<RL<1) , indicating that the adsorption of Fe^{3+}/Fe^{2+} onto the PKSAC was a favorable process and also confirm the suitability of Langmuir model to describe the equilibrium data.

3.4.3 Freundlich model

Freunlich model, as mathematically expressed in equations 2a and 2b, was also applied to analyze the equilibrium data. This was carried out by plotting a linear relationship of $\boldsymbol{lnq_e}$ and $\boldsymbol{C_e}$. The Freundlich constants, $\boldsymbol{K_F}$ and n values were obtained from the intercept and slope of the curve respectively. From The linear plot, presented in Fig. 6. R^2, K_F and n values at various temperature values were determined and shown on Table 3. With the R^2 value of 0.96, Freunlich model described the equilibrium adsorption data better at 40ºC . Values of n for all the temperature values under study were within the range of between 0 and 1 suggesting heterogeneity of PKSAC surface. The least n value recorded at temperature value of 40ºC indicated adsorption favorability [18,42] and also implied that PKSAC surface was more heterogeneous at that temperature. This observation buttressed the axiom that adsorption surfaces become more heterogeneous as n value tends to zero [62]. On the nature of adsorption, Freunlich model confirmed the adsorption of Fe^{3+}/Fe^{2+} onto PKSAC chemisorptions as n values were less than unity [63].

Table 3. Parameters of Temkin, Langmuir and Fraunlich models calculated at various temperature values

Isotherms	Models	25ºC	40ºC	80ºC
Temkin *constants*				
b_T	$q_e = \frac{RT}{b_T} lnA_T + \frac{RT}{b_T} lnC_e$	6.08x10^{-4}	0.001	5.22x10^{-4}
A_T		1.006	1.005	1.001
R^2		0.87	0.92	0.89
Langmuir *constants*				
q_{max}	$\frac{C_e}{q_e} = \frac{1}{K_L q_{max}} + \frac{1}{q_{max}} C_e$	203.9	389.3	380.1
K_L		5.71	8.51	7.24
R^2		0.87	0.95	0.90
RL		0.012	0.017	0.015
Freundlich *constants*				
K_F	$lnq_e = lnK_F + \frac{1}{n} lnC_e$	5.81	6.76	7.84
n		0.85	0.63	0.95
$R2$		0.72	0.96	0.73

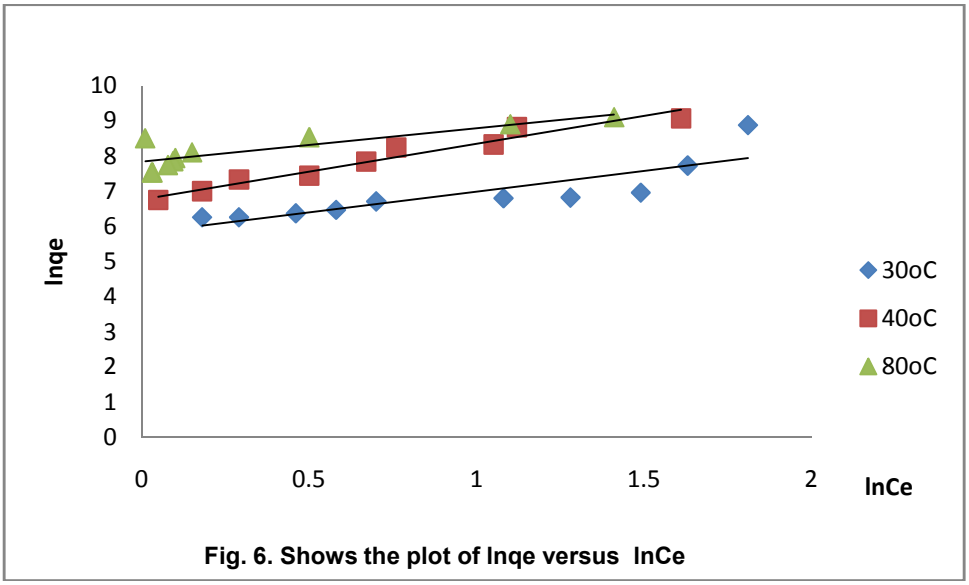

Fig. 6. Shows the plot of lnqe versus lnCe

3.3.4 Temkin model

To further evaluate the adsorption potentials of PKSAC for Fe^{3+}/Fe^{2+}, Temkin adsorption isotherm models shown in equations 4a and 4b were adopted. The temkin isotherm plot made by q_e Vs lnC_e for the three temperature values under study were presented in Fig. 7 and the isotherm parameters, b_T and A_T calculated from the slope and intercept of the plot respectively were shown on Table 3. The Temkin constants b_T and A_T showed apparent variations with temperature. b_T which gives impression of heat of sorption and binding energy increased from 6.08x10^{-4} at temperature of 25ºC to 0.001 at 40ºC but decreased to 5.22x10^{-4} at 80ºC. At 40ºC the binding energy holding Fe^{3+}/Fe^{2+} to PKSAC were strong suggesting high adsorption affinity, whereas at 80ºC heat of adsorption and binding energy were on the decline implying low adsorption, low coverage and possible desorption due to

temperature increase [64]. A_T values assumed the same trend of temperature variation with that of b_T , buttressing the fact that adsorption capacity of the adsorbent was higher at 40ºC than at 80ºC. With the prevailing condition, the possibility was that the adsorbent-adsorbate interaction related to Temkin model must be low at 80ºC [65] leading to low adsorption potential. Also, Correlation coefficient, R^2 varies with temperature as represented in Table 3. The correlation coefficients were reasonably high but recorded the highest value at 40ºC.

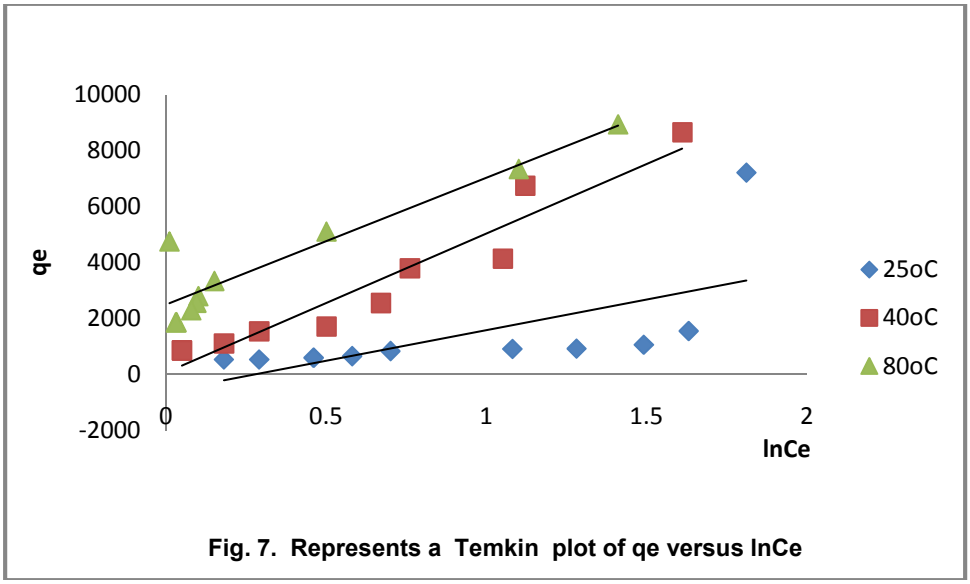

Fig. 7. Represents a Temkin plot of qe versus lnCe

3.5 Adsorption Kinetic Study

To understand the interaction of Fe^{3+}/Fe^{2+} with PKSAC and to predict their fate with time, the following adsorption kinetic models were adopted; pseudo-first, second order kinetics, power-function, Elovick and intra-diffusion equation.

3.5.1 Pseudo-first order equation

Plots of $\boldsymbol{log(q_e - q_t)\ Vs\ t}$ shown in Fig. 8 for various temperature values under study gave linear curves. The relationship between the plotted variables was generally not strong as all the R^2 values were below 0.9. From the results on Table 4, R^2 varied with temperature, the correlation value (R^2) was highest at temperature value of 40ºC followed by that of 25ºC and the least value was observed at 80ºC. Low value of R^2 recorded at the highest temperature of 80ºC showed that the first order kinetic equation does not provide a good model for the adsorption of Fe^{3+}/Fe^{2+} onto PKSAC at that temperature. K_1 equally varied linearly with temperature.

The highest K_1 value observed at 80ºC indicated a low uptake of Fe^{3+}/Fe^{2+} onto the PKSAC. This implies reduction in adsorption rate due to lose binding energy holding Fe^{3+}/Fe^{2+} to PKSAC and that of solubility of Fe^{3+}/Fe^{2+} in bulk solution occasioned by increase in temperature [24,66].

3.5.2 Second order kinetic

The Second order kinetic as presented in equations 7a and 7b was also adopted for the kinetic study. A plot of $\frac{t}{q_e}$ Vs t presented a linear curve shown on Fig. 9, with substantially high R^2 values for all the temperature values, suggested that the adsorption of Fe^{3+}/Fe^{2+} was better represented by the second-order kinetic model than the first-order model.. The rate constant of second – order adsorption (k_2) was found to be lower than that obtained for the pseudo- first order model. This observation showed faster uptake of Fe^{3+}/Fe^{2+} onto the PKSAC and favorable as described by the model [67]. The R^2 values at various temperature ranges were shown on Table 4

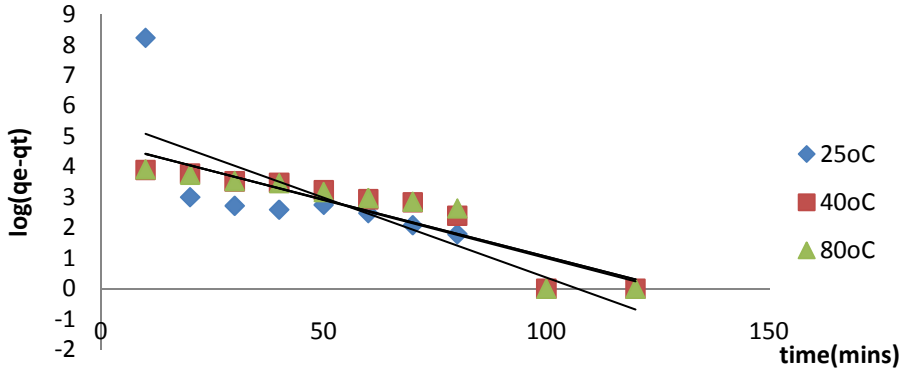

Fig. 8. Pseudo -first order kineticsfor the adsorption process

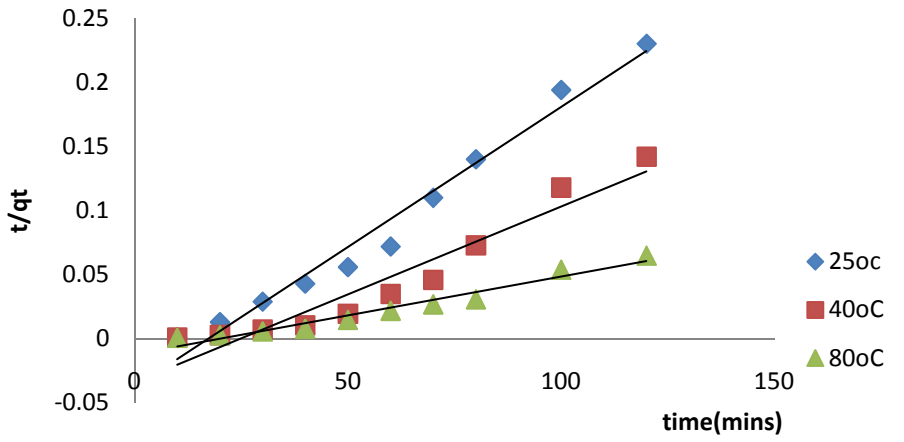

Fig. 9. Second order kinetics for the adsorption adsorption peocess

Table 4. Adsorption Kinetic Parameters of the Adsorption Process

Models	Equations	Linear	25ºC	40ºC	80ºC
Lagergren	$\frac{dq_t}{dt} = K_1(q_e - q_t)$	$\log(q_e - q_t) = logq_e - \frac{K_1}{2.303}t$			
Lagergren constants					
K_1			0.074	0.088	0.11
R^2			0.69	0.86	0.68
Second –order	$\frac{dq_t}{dt} = K_2(q_e - q_t)^2$	$\frac{dq_t}{dt} = \left(\frac{1}{K_2 q_e^2}\right) + \left(\frac{1}{q_t}\right)t$			
Second –order constants					
K_2			0.002	0.004	0.0049
R^2			0.98	0.93	0.96
Power- Function	$q_t = at^b$	$logq_t = loga + blogt$			
Power- Function constants					
a			0.714	0.743	0.861
b			4.74	6.87	3.69
R^2			0.97	0.99	0.96
Elovick	$\frac{dq_t}{dt} = aexp(-\beta q_t)$	$q_t = \frac{1}{\beta}\ln \alpha\beta + \frac{1}{\beta}\ln t$			
Elovick constants			1.54	2.54	1.35
α			0.52	0.154	0.76
β			0.64	0.96	0.97
R^2					
Intra-particle Diffusion Constants	$q_t = K_t t^{0.5}$	$logq_t = K_t + \frac{1}{2}logt$			
K_t			690.1	997.1	719.9
R^2			0.86	0.87	0.80

3.5.3 Power function

Power function model was adopted to describe the adsorption kinetic data of this study. The model is as expressed in equations 8a and 8b. To test the suitability of the model to the data, a plot of $\boldsymbol{logq_t}$ Vs $\boldsymbol{blogt}$ was made and presented in Fig. 10. The plots made at various temperature values of 25ºC, 40ºC and 80ºC produced linear curves with a and b as the power function constants. Values of correlation coefficients (R^2) and the power function constants for the three temperature values were shown on Table 4. These values showed some variations with temperature. At temperature of 80ºC which seemed to be the temperature of least adsorption value (as observed previously), power function constant ''a'', has the least value compared with that of other temperature values. As power constant ''a'' indicates the adsorption and or desorption rate of the pollutants [68,69], it was then implied that the rate of adsorption was minimal at temperature of 80ºC and highest at 40ºC. Regarding the fitness of the kinetic data the correlation coefficient recorded 0.97,0.99 and 0.95 for 25ºC, 40ºC and 80ºC respectively indicated that power function described the data better than described by pseudo- first order and second-order models.

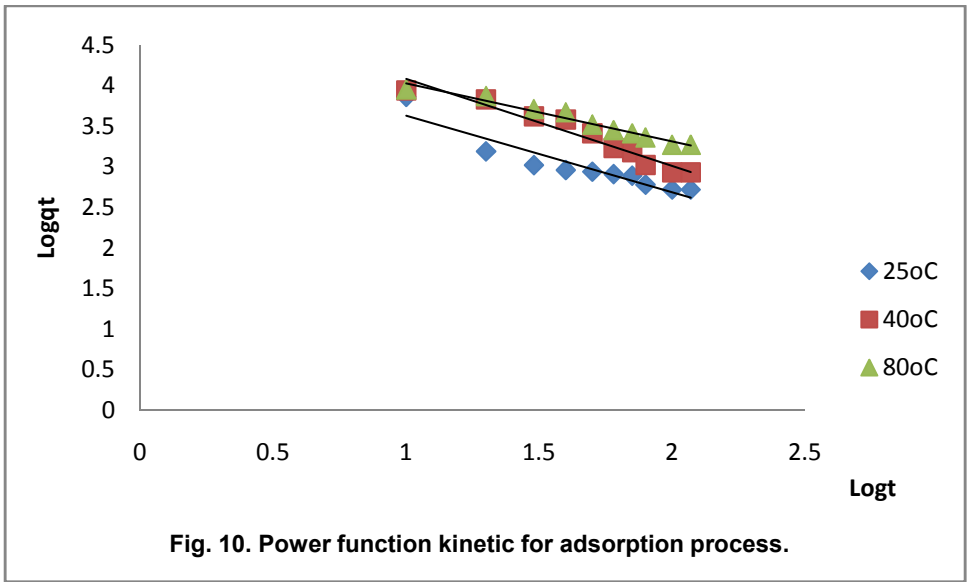

Fig. 10. Power function kinetic for adsorption process.

3.5.4 Elovich kinetic model

Kinetic study of adsorption of Fe^{3+}/Fe^{2+} onto PKSAC was further carried out using Elovich kinetic model and was presented in Fig. 11. The results of the study for the study temperature values indicated that the plots of $\boldsymbol{q_t}$ Vs $\boldsymbol{lnt}$ were linear over the whole time range. The Elovick constants, α and β which characterize the adsorption and desorption rates of process respectively were calculated and presented on Table 4. It was observed that the values of the Elovick constants were sensitive to temperature variation. Lowest value of 'α' was observed at the highest temperature of 80ºC showing low Fe^{3+}/Fe^{2+} uptake rate. Researchers attributed this to the following; (1) desorption tendency of Fe^{3+}/Fe^{2+} at high temperature [49] and (2) increase in oscillation of binding energy of Fe^{3+}/Fe^{2+} occasioned by high temperature[70]. The low uptake rate at high temperature was further substantiated by increase in value of β at high temperature which indicated high rate of desorption due to rise in temperature [42]. Correlation coefficients were also deduced from

the curve and the values equally shown on the table. From the values of R^2 observed, Elovick model reasonably described the adsorption data but not as sufficient as described by the power function and second- order model.

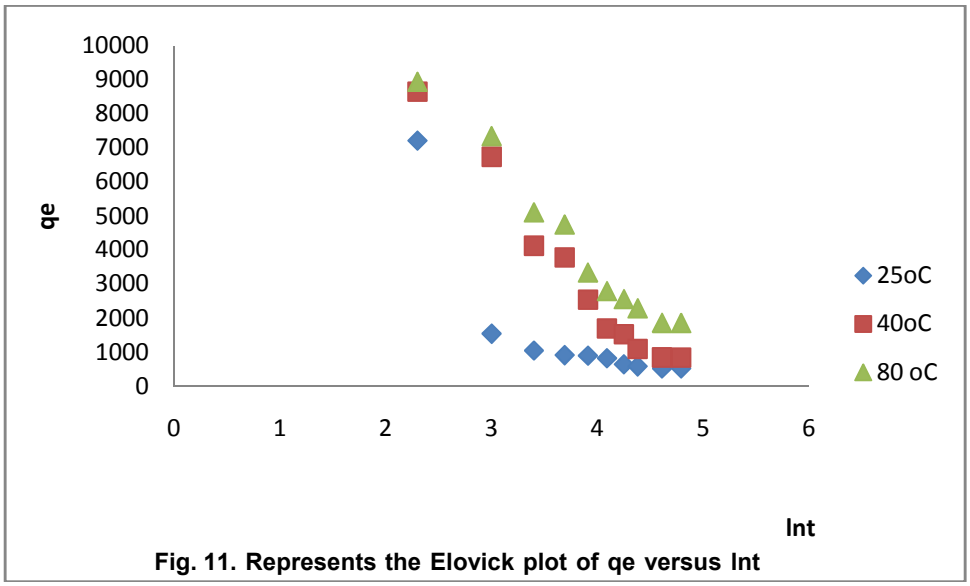

Fig. 11. Represents the Elovick plot of qe versus lnt

3.5.5 Intra diffusion kinetic model

In order to determine the adsorption steps of this study, intra-particle diffusion(diffusion of solute molecules into the interior of the pores) as presented in equations 10a and 10b was used. A plot of q_t Vs $t^{0.5}$ produced a linear curve shown in Fig. 12 where K_t was calculated from the slope and its values for various temperature values shown on Table 4. The correlation coefficients (R^2) were equally presented on the table. Temperature variation has pronounced effects on K_t values. The intra-diffusion constant, K_t increased with temperature but reduced at temperature of 80ºC. This observation suggested that the adsorption capacity of PKSAC was low at that temperature. The linear plot not passing through the origin confirmed the possibility of less influence of intra-particle diffusion of Fe^{3+}/Fe^{2+} into the pores of the adsorbent, PKSAC at the initial stage of the adsorption process. From equation 10b, K_t varies directly with equilibrium concentration, q_e and square root of the diffusion coefficient, D. Although intra-particle diffusion not wield much influence on this adsorption process, the prevailing condition implies that K_t determined the diffusion of Fe^{3+}/Fe^{2+} molecules into the interior of the PKSAC pores.

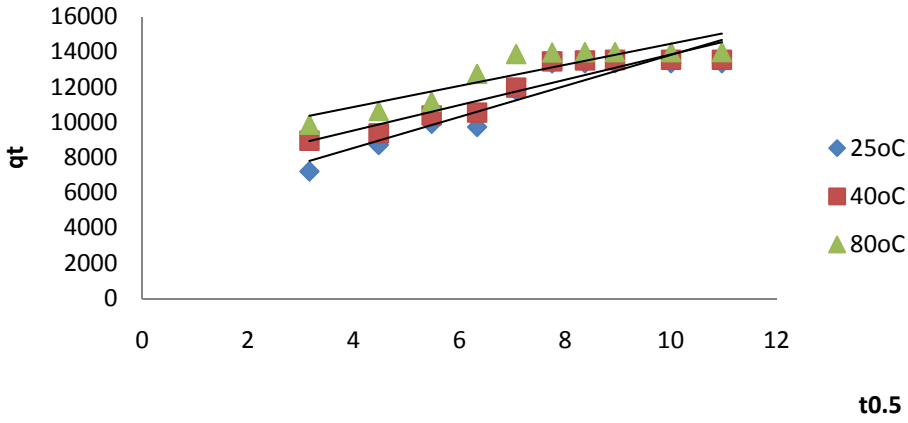

Fig. 12. Intra-diffusion kinetic model for the adsorption process

To further decide the rate controlling step, liquid diffusion model expressed in equation 10c was employed where $\boldsymbol{ln(1-\alpha)}$ Vs t was ploted and the plot yielded a linear curve without passing through the origin,(see Fig. 13). This signified that the mass transfer of Fe^{3+}/Fe^{2+} through the liquid film onto the PKSAC took place before the intra-particle diffusions of the pollutant molecules. Several researchers observed similar trend in their various studies [38,44,71].

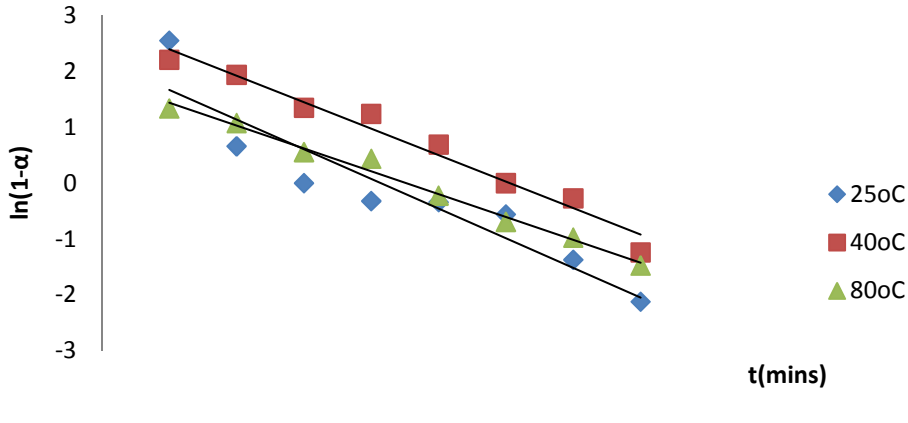

Fig.13. Liquid diffusion model for the adsorption process

3.6 Thermodynamic Study

3.6.1 Activation energy of adsorption

The average rate constants of adsorption(Kad) was determined at each temperature values of 25ºC, 40ºC, and 80ºC by computing the quotient of the amount of Fe^{3+}/Fe^{2+} adsorbed at various time of adsorption. With the Arrhenius model, a plot of $\boldsymbol{lnK_{ad}\ Vs\ \frac{1}{T}}$ was made. From the slope and the intercept of the linear curve presented in Fig. 14 the energy of activation, $\boldsymbol{E_a}$ and frequency of collision, lnA respectively were derived. The rate constant as a function of temperature showed that the rate of Fe^{3+}/Fe^{2+} adsorption on PKSAC adsorbent increased with increase in temperature. This confirmed the following observations of other researchers; (I) That increase in temperature increased the active sites of the adsorbent therefore providing more sites for adsorption. (ii) That high temperature equally decreased the thickness, resulting to outright rupture of the barrier surrounding the adsorbent with increasing mass transfer of the adsorbate [51,20,72] and (iii) increase in bulk motion of the adsorbate towards the adsorbent [16]. The activation energy and frequency of collision were calculated as 0.8017KJ/mol and $\boldsymbol{8.1\ x\ 10^{-5}\frac{mg}{g}/s}$ respectively.The thermodynamic study was further carried out at various temperature values using the other thermodynamic parameters which include ; Gibb-free energy (ΔG^o), Enthalpy(ΔH) and Enthropy (ΔS) of adsorptions. Enthalpy was determined from the slope of Van't Hoff plot of $\boldsymbol{\frac{\Delta G^o}{T} Vs\ 1/T}$ presented in Fig. 15 while the (ΔG^o) and (ΔS^o) were calculated from equations 12 and 13b respectively. The values of the three thermodynamic parameters were negative, confirming that the interaction of Fe^{3+}/Fe^{2+} with PKSAC was product-favoured . This implied that the adsorption of Fe^{3+}/Fe^{2+} onto PKSAC increased with higher negative thermodynamic parameters. For instance, the negative values of the Gibbs free energy(the available energy for the adsobate and adsorbent) showed that the energy was released into the environment to produce the negative Enthalpy and Enthropy of the process [31,68]. Also, decrease in the values of $\boldsymbol{\Delta G^o}$ at increasing temperature indicted spontaneity of Fe^{3+}/Fe^{2+} adsorption on the adsorbent. The negative values of $\boldsymbol{\Delta H^o}$ and $\boldsymbol{\Delta S^o}$, indicated the exothermic nature and decreasing randomness of adsorbate / adsorbent interface during Fe^{3+}/Fe^{2+} adsorption on PKSAC respectively. This conditions provided ample opportunity for adequate adsorption of Fe^{3+}/Fe^{2+} onto the adsorbent. For instance, the exothermic condition due to high negative Enthalpy, enhanced the mobility of Fe^{3+}/Fe^{2+} in the bulk solution leading to high adsorption with its attendant increase in binding strength of the adsorbate to the adsorption sites [69]. Also, the steady and definite arrangement of the adsorbate / adsorbent interface occasioned by decrease in adsorption Enthropy, provided straight course for Fe^{3+}/Fe^{2+} towards adsorption. With this axiom it therefore implied that the affinity of Fe^{3+}/Fe^{2+} to PKSAC was high and was higher at higher negative values of Enthalpy of adsorption as shown on Table 5.

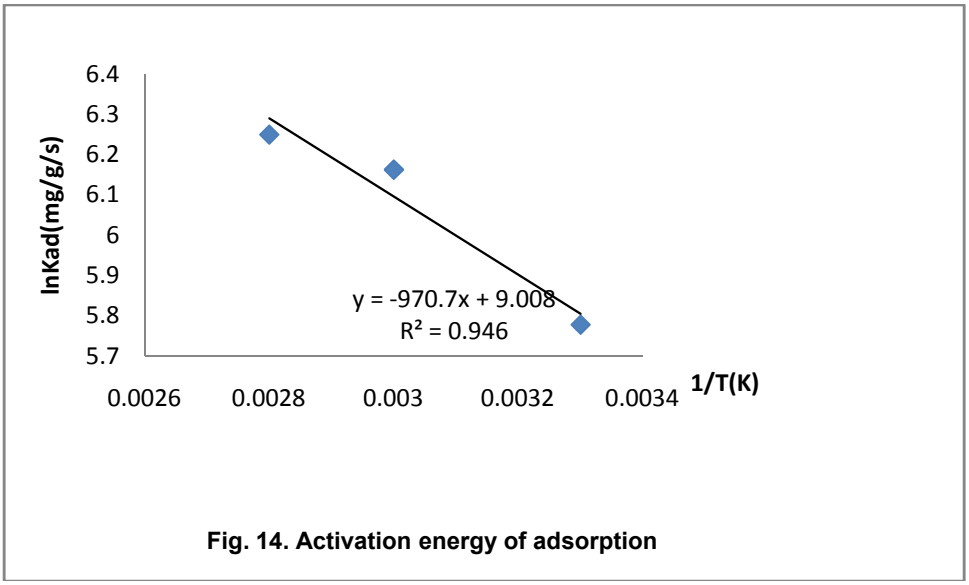

Fig. 14. Activation energy of adsorption

Table 5. Thermodynamic Parameters of the Adsorption Process

Temperature K	ΔG^o	$\Delta S^o = \frac{\Delta H^o - \Delta G^o}{T}$	ΔH^o
298	-4.35	-7.88	-2341.39
313	-5.60	-7.86	-2459.24
353	-5.50	-7.84	-2773.57

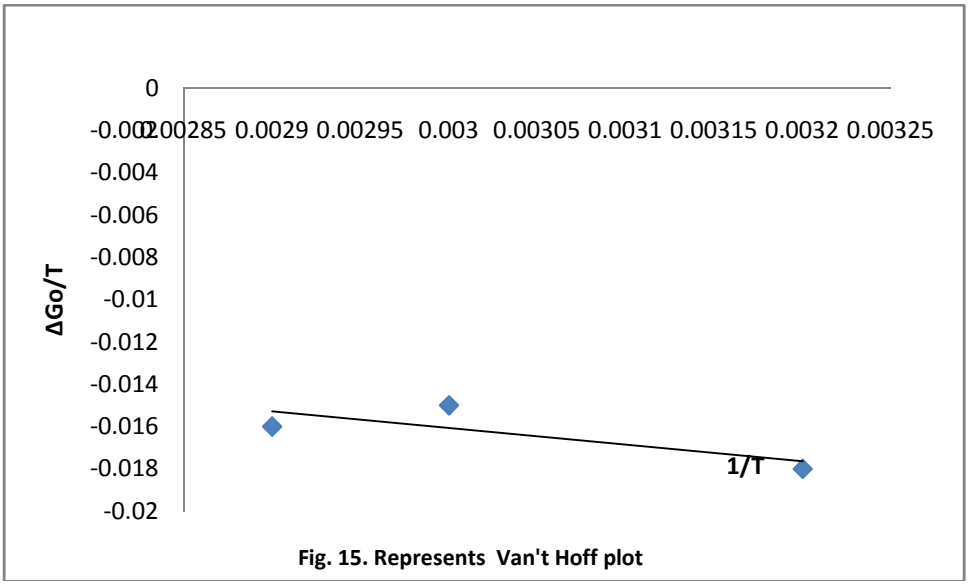

Fig. 15. Represents Van't Hoff plot

4. CONCLUSIONS

Fe^{3+}/Fe^{2+} adsorption of a shallow well water, onto palm kernel shell activated carbon (PKSAC) adsorbent was studied in batch experiment. Percentage removal increased with increased adsorbent loading, temperature and Fe^{3+}/Fe^{2+} concentration decrease. Removal efficiency got to equilibrium at optimal temperature of 80ºC. Also, removal efficiency increased progressively with contact time till the optimum time of 100 minutes.

The adsorption isotherm models was adopted to test the relevance of these models to the equilibrium experimental data. The models fitted the data in this order; Langmuir > Temkin>Freunlich. The values of the dimensionless separation factor calculated from Langmuir constant confirmed favorable adsorption of Fe^{3+}/Fe^{2+} onto PKSAC adsorbent. Langmuir adsorption capacity of the adsorbent studied at three temperature values of 25ºC, 40ºC and 80ºC increased from 203.9mg Fe^{3+}/Fe^{2+}/g to 389.3 mg Fe^{3+}/Fe^{2+}/g when the temperature increased from 25ºC to 40ºC. Adsorption capacity decreased to 308.1 mg Fe^{3+}/Fe^{2+}/g at temperature of 80ºC.

The kinetic of adsorption study with First-order, Second-order, Power-function, Elovick and Intra-diffusion models showed that the models reasonably described the data. Variations were observed on the extent at which the kinetic models described the data and that was ranked in this order; power-function>second-order>Elovick>intra-diffusion>first-order kinetics. For the rate controlling step of the adsorption, mass transfer predominated the adsorption as Fe^{3+}/Fe^{2+} transferred through the liquid film diffusion onto PKSAC before the intra-particle diffusion.

Thermodynamic parameters ($\Delta \boldsymbol{G^o}$, $\Delta \boldsymbol{H^o}$ and $\Delta \boldsymbol{S^o}$) obtained at various temperature values showed favorability of adsorption of Fe^{3+}/Fe^{2+} onto PKSAC. $\Delta \boldsymbol{H^o}$ was negative at all temperature levels indicating exothermic process but the highest negative value was observed at temperature of 40°C equally implying highest favorability of adsorption of Fe^{3+}/Fe^{2+} at that temperature. Decrease in the values of $\Delta \boldsymbol{G^o}$ (High negative values) at increasing temperature indicted spontaneity of Fe^{3+}/Fe^{2+} adsorption on the adsorbent. The high negative value of $\Delta \boldsymbol{S^o}$ implied decreasing randomness of adsorbate / adsorbent interface during Fe^{3+}/Fe^{2+} adsorption on PKSAC. Randomness of Fe^{3+}/Fe^{2+}/PKSAC interface decreased most at 80ºC, implying low adsorption at that temperature. Activation energy of adsorption increased with temperature.

COMPETING INTERESTS

Authors have declared that no competing interests exist.

REFERENCES

1. Joseph W, Stucki, Kangwon Lee, Lingzhi Zhang, Richard A. Larson. Effects of iron oxidation state on the surface and structural properties of smectites. Pure Appl. Chem. 2002;74(11):2145–2158.
2. David B. Vance. Iron - the environmental impact of a universal element: National Environmental Journal. 1994;4(3):24-25.
3. Xu JC, Sims GK, Kostka JE, Wu J, Stucki JW. Environ. Toxicol. Chem. 2001;20:2717–2724.

4. Favre FD, Tessier M, Abdelmoula JM, Genin WP, Gates P. Boivin. Eur. J. Soil Sci. 2002;53(2):175–183.
5. Dallman PR. Iron. In: Brown ML, ed. Present knowledge in nutrition, 6th ed. Washington, DC, International Life Sciences Institute, Nutrition Foundation. 1990. J Therm Anal Calorim. 2010;101:785–794.
6. Elinder CG. Iron. In: Friberg L, Nordberg GF, Vouk VB, eds. Handbook on the toxicology of metals, Amsterdam, Elsevier. 1986;2:276-297.
7. Ottawa RO. Nutrition recommendations. The report of the Scientific Review Committee. Department of National Health and Welfare (Canada); 1990.
8. Minnesota Pollution Control Agency, Environmental Outcomes Division Ground Water Monitoring & Assessment Program report; 1999.
9. El-Geundi SM. “Colour Removal from Textile Effluents-by Adsorption Techniques” Water Res. 1991;25:271-273.
10. Goswami S, Ghosh UC. Studies on Adsorption Behaviour of Cr (VI) Onto Synthetic Hydrous Stannic Oxide. Water SA. 2005;31(44):57-602.
11. Aksu Z. Application of Biosorption of removal of Organic Pollutants: A Review. Process Biochemistry. 2005;40(3-4):997-1026.
12. Mohammad ME, Muttucumaru S. Review of pollutant Removed by Electrocoagulation and Elcetroagulation/Flotation Processes,” Journal of Environmental Management. 2009;90(5)1663-1679.
13. Elmorsi T M, Riyad YM, Mohamed ZH, Abd El Bary HM. “Decolorization of Mordanedt red 73 azo.Dye in Water Using H2O2/UV and Photo-Fenton Treat-ment,” Journal of Hazardous Materials, Vol. 2010;174(1-3):352-358.
14. Karithikayan S, Gupta VK, Boopathy R, Titus A, Sekaran G. A new approach for the degradation of high concentration of aromatic amine by heterocatalytic fenton oxidation ; Kinetic and spectroscopic studies. J molecular liquid. 2012;173(2):153-163.
15. Gupta VK, Imran Ali, tawfik salah, Arunima Nayak, Shipi Agarwai. Chemical treatment technologies for wastewater recycling; An overview. RSC Advance 26380-6388; 2012.
16. Tawfik, Saleh A, Gupta VK. column with CNT/Magnesium oxide composite for lead(II) removed from water. Env. Sci. and pollution research. 2012;19(4):1224-1228.
17. Gupta VK, Rajeev Jain, Alok Mittel, Megha Mathur, Shalini Sikanwar. Photochemical degradation of the hazardous dye safranin-T using Tio2 catalyst. J. Colliod and interface science. 2007;309(2):464-469.
18. Bulut Y Gozubenli N, Aydın H. “Equilibrium and Kinetics Studies for Adsorption of Direct Blue 71 from Aqueous Solution by Wheat Shells,” Journal of Hazard-ous Materials. 2007;144(1-2)300-306.
19. Alok Mittal, Lisha Kump (Krishman), vinod, K. Gupta. Use of waste material- Bottom Ash and De-oiled soya as potential adsorbent of Amaranth from Aqueous solutions. Journal of hazardous materials. 2005;117:171-178.
20. Khani MH, Keshitak AR, Ghannadi M, pahlavanzadah H. Equilibrium, Kinetic and thermodynamic study of the biosorption of uranium onto Cystoseira indica algae. Journal of hazardous material. 2007;170:612-625.
21. Lakshmipathiraj P, Narasimhan BRV, Prabhakar S Bhaskar Raju G. Adsorption studies of Arsenic on Mn-subtituted iron oxyhydroxide. journal of colloid interface science. 2006;304:317-322.
22. Nigamananda Das, Ranajiut Kumar Jana. Adsorption of some bivalent Haevy metals ions from aqueous solution by Manganese nodule leached residues. 2006;293:253-262.
23. Brandt A, Bu¨low M, Derylo-Marczewska A, Goworek J, Schmeißer J, Scho¨ps W, Unger B. Novel zeolite composites and consequences for rapid sorption processes. Adsorption. 2007;13:267–79.

24. Gupta VK, Alok Mittal, Lisha Krishnan, Jyoti mittal. Adsorption treatment and recovery of the hazardous dye; brilliant blue FCF over bottom ash and de-oiled soya. J. Colliod and interface science. 2006;293(27):16-26.
25. Alok Mittal, Jyoti mittal, Artimalviya dipika kaur, Gupta VK. Adsorption of hazardous dye crystal violet from waste materials. J.Colliod interface science. 2010;343(2):463-473.
26. Gupta VK, Rajeev jain, shally Varshey. Removal ofreactofix golden yellow 3 RFN from aqueous solution using wheat husk; An agricultural waste. J. hazardous material. 2007;142(2):443-448.
27. Alok mittal, Gupta VK, Artimalviya, Jyoti mittal. Process development for the batch and bulk removal and recovery of a hazardous, water soluble Azo dye (metani yellow) by adsorption over waste materials (bottom ash de-oiled soya. J. Hazardous materials. 2008;151(2):821-832.
28. Gupta VK, Arshi Rastogi, Arunima Nayak. Biosorption of nickel unto treated algae (oedogonium hatei). Application of isotherm and kinetic models. J.colliod interface science. 2010;342(2):533-539.
29. Emmanuel A, Oluyemi, Adewale F, Adeyemi, Iyabo O, Olabanji. Removal of pb2+ and cd2+ ions from wastewaters using palm kernel shell charcoal (PKSC) Research Journal in Engineering and Applied Sciences, Emerging Academy Resources. 2012;1(5):308-313.
30. Ademiluyi FT, David-West EO. Effect of Chemical Activation on the Adsorption of HeavyMetals Using Activated Carbons fromWasteMaterials International Scholarly Research Network. ISRN Chemical Engineering; 2012.
31. Taha M, Elmorsi. Equilibrium Isotherms and Kinetic Studies of Removal of Methylene Blue Dye by Adsorption onto Miswak Leaves as a Natural Adsorbent Journal of Environmental Protection. 2011;2:817-827.
32. Annadurai G. and Krishnan M.R.V. Adsorption of basic dye on chitin, Indian J. Environ. Protection. 1996;16:444-449.
33. Verma VK, Mishra AK. Dye removal by Sawdust based adsorbent, Pollution Research. 2005;24(1):97-99.
34. Guo J, Lua AC. Characterization of chars pyrolysed from oil palm stones for preparation of activated carbons. Journal of Analytical and Applied Pyrolysis. 1998;46(2):113. .
35. Guo J, Lua AC. Preparation and characterization of adsorbents from oil palm fruit solid waste. Journal of Oil Palm Research Malaysian Palm Oil Board. 2000;12:64-70.
36. Panida Sampranpiboon, Pisit Charnkeitkong. Equilibrium Isotherm, Thermodynamic and Kinetic Studies of Lead adsorption onto. pineapple and paper waste sludges. International journal of energy and environment. 2010;3:4.
37. Nader Yousefi, Ali Fatehizadeh, Elham Azizi, Mohammad Ahmadian, Abdolkarim Ahmadi, Ahmad Rajabizadeh, Ali Toolabi. adsorption of reactive black 5 dye onto modified wheat straw:isotherm and kinetics study Sacha Journal of Environmental Studies, Volume 1 Number. 2011;2:81-91.
38. Saeed A, Akhter MW, Iqbal M. Removal and recovery of heavy metals from aqueous solution using papaya wood as a new biosorbent. Sep. Purify. Technol. 2005;45:25-31.
39. Foo KY, Hameed BH. Insights into the modeling of adsorption isotherm systems. Chemical Engineering Journal. 2010;156:2–10.
40. Vijayaraghavan K , Padmesh TVN, Palanivelu K, Velan M. Biosorption of nickel(II) ions onto Sargassum wightii: application of two-parameter and three parameter isotherm models, J.Hazard. Mater. 2006;B133:304–308.

41. Kundu S. Gupta AK. Arsenic adsorption onto iron oxide-coated cement (IOCC): regression analysis of equilibrium data with several isotherm models and their optimization, Chem. Eng. J. 2006;122:93–106.
42. Pérez-Marín AB, Meseguer Zapata V, Ortuno JF, Aguilar M, Sáez J, Llorens M. Removal of cadmium from aqueous solutions by adsorption onto orange waste, J. Hazard. Mater. 2007;B139:122–131.
43. Webber TW, Chakkravorti RK. Pore and solid diffusion models for fixed-bed adsorbers, AlChE J. 1974;20:228–238.
44. Badmus MAO, Audu TOK, Anyata BU. Removal of lead ion from industrial wastewater by activated carbon prepared from periwinkle shells. Turkish journal of engineering and environmental science. 2007;31:251-263.
45. Moore JW, Conrad LS, Peter CJ. Chemistry, the molecular science. Third edition David Harris publishers USA. 2005;692-693.
46. Ho YS, McKay G. "Pseudo-Second Order Model for Sorption Processes," Process Biochemistry. 1999;34(5):735-742.
47. Hameed BH, Din ATM, Ahmad A L. "Adsorp-tion of Methylene Blue onto Bamboo-Based Activated Carbon: Kinetics and Equilibrium Studies," Journal of Hazardous Materials. 2007;141(3):819-825.
48. Alzaydien A S. "Adsorption of Methylene Blue from Aqueous Solution onto a Low-Cost Natural Jordanian Tripoli," American Journal of Applied Sciences. 2009;5(1):197-208.
49. Glenda M. Herman, Extension Housing Specialist Iron and Manganese in Household Water Published by: North Carolina Cooperative Extension Service Publication Number: HE-394 . Last Electronic Revision; March 1996(JWM).
50. Oladoja NA, Aboluwoye CO, Oladimeji YB. Kinetics and Isotherm Studies on Methylene Blue Adsorption onto Ground Palm Kernel Coat. Turkish J. Eng. Env. Sci. 2008;32:303 – 312.
51. Bhattacharyya KG, Sharma A. "Kinetics and Thermodynamics of Methylene Blue Adsorption on Neem Leaf Powder" Dyes and Pigments. 2005;65:51-59.
52. HoYS, Ofomaja AE. "Kinetics and Thermodynamics of Lead Ion Sorption On Palm Kernel Fiber From Aqueous Solution" Process biochemistry. 2005a;40:3455-3461.
53. Grluk M, Hubicki Z. "Kinetics; isotherm and thermodynamic studies of Reactive Black5 removal by acid acrylic resins." chemical Engineering. 2010;162:919-926.
54. Adam W. Marczewski Anna Deryło-Marczewska Agata Słota. Adsorption and desorption kinetics of benzene derivatives on mesoporous carbons. Adsorption. 2013;19:391–406.
55. Garg A, Gupta VK, Yadav RB, Kumar R. Removal of acid dyes by low cost adsorbent, Bioresour. Technology. 2003;89:121-124.
56. Le Zeng. Arsenic Adsorption from Aqueous Solutions on an Fe(III)-Si Binary Oxide Adsorbent Water Qual. Res. J. Canada. 2004;39(3):267–275.
57. Demirbas E M, Kobya AES, Konukman. Error analysis of equilibrium studies for the almond shell activated carbon adsorption of Cr (VI) from aqueous solutions, J. Hazard. Mater. 2008;154:787–794.
58. Rounak M, Shariff. Kinetic & Thermodynamic Study for Adsorption– Desorption of Diazinon with Copper in The Presence of Surfactant. Global Journal of Science Frontier Research Chemistry. 2012;12:4.
59. Kavak D. "Removal of Boron from Aqueous Solutions by Batch Adsorption on Calcined Alunite Using Experi-mental Design," Journal of Hazardous material. 2009;63(1)308-314.
60. Hameed BH. "Grass Waste: A Novel Sorbent . Removal of Basic Dye from Aqueous Solution," Journal of Hazardous Materials. 2009;166(1):233 -238.

61. Allen SJ, Mckay G, Porter JF. Adsorption isotherm models for basic dye-adsorption by peat in single and binary component systems, J. Colloid InterfaceSci. 2004;280:322–333.
62. Derylo-Marczewska AM, Blachnio AW, Marczewski A, Swiatkowski B, Tarasiuk. Adsorption of selected herbicides from aqueous solutions on activated carbon, J. Therm Anal Calorim. 2010;101:785–794.
63. Haghseresht F Lu G. Adsorption characteristics of phenolic compounds onto coal-reject-derived adsorbents, Energy Fuels. 1998;12:1100–1107.
64. Shahmohammadi-Kalalagh Sh, Babazadeh H, Nazemi AH, Manshouri M. Isotherm and Kinetic Studies on Adsorption of Pb, Zn and Cu by Kaolinite Caspian J. Env. Sci. 2011;9(2):243-255.
65. Bose P, Bose MA, Kumar S. Critical evaluation of treatment strategies involving adsorption and chelation for wastewater containing copper, zinc, and cyanide. Adv.Environ. Res. 2002;7:179–195.
66. Bansal RC, Goyal M. Activated Carbon Adsorption, Boca Raton, Crc Press Taylor Francis Group; 2005.
67. Chen DZ, Zhang JX, chen JM. Adsorption of methyl tert-butyl ether using granular activated carbon equlilibrium and kinetic analysis. Int. J. Environmental science tech. 2011;7(2):235-242.
68. Manna BR, Dey S, Debnath S, Ghosh UC. Removal of arsenic from groundwater using crystalline hydrous ferric oxide (CHFO). Water Qual. Res. J. Canada. 2003;38(1):193–210.
69. Gupta VK. Equilibrium uptake, sorption dynamics, process development, and column operations for the removal of copper and nickel from aqueous solution and wastewater using activated slag, a low-cost adsorbent.Ind. Eng. Chem. Res. 1998;37:192–202.
70. Ho YS, Wase DAJ, Forster CF. Removal of lead ions from aqueous solution using sphagnum moss peat as adsorbent. Water SA. 1996;22(3):219-224.
71. Nouri L Ghodbane I, Hamdaoui O, Chiha M, Batch sorption dynamics and equilibrium for the removal ofcadmiumions from aqueous phase using wheat bran, J. Hazard. Mater. 2007;149:115–125.
72. Vinod K Gupta, Alok Mittal, Artimdviya Jyoly Mittal. Adsorption of Carmoisine-A from wastewater using waste materials-bottom ash and de-oiled soya. Journal of colloid interface science. 2009;335:24-33.

Peer-review history:
The peer review history for this paper can be accessed here:
http://www.sciencedomain.org/review-history.php?iid=393&id=16&aid=3362